Journal of Solid State Chemistry 184 (2011) 97–103

Contents lists available at ScienceDirect

Journal of Solid State Chemistry

journal homepage: www.elsevier.com/locate/jssc

Crystal and electronic structures of $CaAl_2Si_2$-type rare-earth copper zinc phosphides $RECuZnP_2$ (RE=Pr, Nd, Gd–Tm, Lu)

Peter E.R. Blanchard, Stanislav S. Stoyko, Ronald G. Cavell, Arthur Mar*

Department of Chemistry, University of Alberta, Edmonton, Alberta, Canada T6G 2G2

ARTICLE INFO

Article history:
Received 29 July 2010
Received in revised form
18 October 2010
Accepted 24 October 2010
Available online 5 November 2010

Keywords:
Rare earths
Phosphides
Crystal structure
Electronic structure
XPS
Magnetic properties

ABSTRACT

The quaternary rare-earth phosphides $RECuZnP_2$ (RE=Pr, Nd, Gd–Tm, Lu) have been prepared by reaction of the elements at 900 °C, completing this versatile series which forms for nearly all RE metals. They adopt the trigonal $CaAl_2Si_2$-type structure (Pearson symbol $hP5$, space group $P\bar{3}m1$, Z=1), as confirmed by single-crystal X-ray diffraction analysis on $ErCuZnP_2$ and powder X-ray diffraction analysis on the remaining members. The Cu and Zn atoms are assumed to be disordered over the single transition-metal site. Band structure calculations on a hypothetically ordered $YCuZnP_2$ model suggest a semimetal, with a zero band gap between the valence and conduction bands. This electronic structure is supported by XPS valence band spectra for $RECuZnP_2$ (RE=Gd–Er), in which the intensity drops off smoothly at the Fermi edge. The absence of a band gap permits the electron count to deviate from the precise value of 16 e^- per formula unit, as demonstrated by the formation of a solid solution in $GdCu_xZn_{2-x}P_2$ ($1.0 \le x \le 1.3$), while still retaining the $CaAl_2Si_2$-type structure. Because the Cu 2p XPS spectra indicate that the Cu atoms are always monovalent, the substitution of Cu for Zn leads to a decrease in electron count and a lowering of the Fermi level in the valence band. The magnetic susceptibility of $RECuZnP_2$ (RE=Gd–Er), which obeys the Curie–Weiss law, confirms the presence of trivalent RE atoms.

1. Introduction

Many ternary intermetallic phases of the form AB_2X_2 adopt either the tetragonal $ThCr_2Si_2$-type or the trigonal $CaAl_2Si_2$-type structure [1]. Phases with the more prevalent $ThCr_2Si_2$-type structure display an exceptionally rich variety of physical properties, including the occurrence of superconductivity in $BaFe_2As_2$ and related compounds [2]. In contrast, relatively less is known about the properties of $CaAl_2Si_2$-type phases, even though they are still quite numerous [3–5]. Among ternary pnictide (Pn) representatives, previous measurements of the electrical and magnetic properties have been made mostly on AB_2Pn_2 (A=Sr, Ba, Eu, Yb; B=Mg, Mn, Zn, Cd; Pn=P, As, Sb), which contain divalent A cations [3k,6]. A recent development is the effort to optimize thermoelectric properties in $SrAl_2Si_2$, $EuZn_2Sb_2$, and related compounds, driven in part by the expectation that they should be small band-gap semiconductors, consistent with the fact that these are charge-balanced and thus Zintl phases [7]. The exceptions are interesting: a few examples (generally the rare-earth (RE) compounds $REAl_2Si_2$ and $REAl_2Ge_2$) seem to violate the requirement for charge balance [8], whereas the eponymous compound $CaAl_2Si_2$, while charge-balanced itself, shows metallic behavior [9]. Following early suggestions about the importance of the electronic structure in stabilizing this structure type [3j], modern theoretical treatments have highlighted electronegativity differences, interlayer interactions, and cation participation as factors in controlling the physical properties of these phases [1,10]. This brief survey indicates that much remains to be learned about the $CaAl_2Si_2$-type phases, despite the considerable and important experimental work that was carried out by Mewis and co-workers years ago [3].

Applying the strategy of aliovalent substitution can afford quaternary $CaAl_2Si_2$-type phases, the rare-earth phosphides $RECuZnP_2$ (RE=Sc, Y, La, Ce, Sm, and Yb) being the few examples previously known [3f,3h,3i,11]. Among these, $SmCuZnP_2$ has been evaluated as a possible infrared transmitting ceramic material [11]. The extent of RE substitution in this incomplete series is unclear and the physical properties of other representatives are unknown. Herein, we report a comprehensive study of $RECuZnP_2$ in which all the missing RE members are now identified and characterized by X-ray diffraction analysis. Magnetic measurements are made on several members of this series and valence-band X-ray photoelectron spectra (XPS), the first on any $CaAl_2Si_2$-type phase, to our knowledge, are reported. The solid solution $GdCu_xZn_{2-x}P_2$ was investigated to determine if the requirement for charge balance can be overcome by gradually changing the electron count as x deviates from 1 in $GdCuZnP_2$.

2. Experimental

2.1. Synthesis

Starting materials were RE pieces (99.9%, Hefa), Cu powder (99.9999%, Cerac), Zn shot (99.99%, Aldrich), and red P powder

* Corresponding author. Fax: +1 780 492 8231.
E-mail address: arthur.mar@ualberta.ca (A. Mar).

0022-4596/$ - see front matter © 2010 Elsevier Inc. All rights reserved.
doi:10.1016/j.jssc.2010.11.001

(99%, Alfa-Aesar). Stoichiometric mixtures of the elements (*RE*+Cu+Zn+2P) were placed in evacuated and sealed fused-silica tubes, which were heated to 500 °C over 1 day, kept at that temperature for 2 days, heated to 900 °C over 1 day, kept at that temperature for 1 week, and then cooled to room temperature over 1 day. The products were reground and reheated with the same temperature program, this procedure being repeated two or three times. The products were analyzed by powder X-ray diffraction (XRD) patterns (Fig. S1 in Supplementary Data) collected on an Inel powder diffractometer externally calibrated to NIST 676a corundum standard. Most products consisted of single-phase *RE*CuZnP$_2$. However, for *RE*=Pr, Nd, Tm, the product contained minor amounts (~6%) of an unidentified phase, whereas for *RE*=Lu, the product contained 20% LuP and 10% of an unidentified phase. Cell parameters for all known members of *RE*CuZnP$_2$, including those previously reported, are listed in Table 1.

Given the disorder between Cu and Zn atoms, it was of interest to determine the solid solubility range, if any. The Gd series was chosen for this purpose. A series of reactions $GdCu_xZn_{2-x}P_2$ ($0.5 \le x \le 1.5$) was conducted with x varying in increments of 0.1 or 0.2, through the same procedure as described above. A phase width of $1.0 \le x \le 1.3$ was established, with the powder XRD patterns revealing single-phase products in this range (Fig. S2 and Table S1 in Supplementary Data).

2.2. Structure determination

Suitably sized single crystals of ErCuZnP$_2$ could be grown with the addition of a single grain of I_2 in the reactions described above. Energy-dispersive X-ray (EDX) analysis confirmed the expected composition (within 5%) of these crystals, with no incorporation of iodine. Intensity data on a selected crystal were collected on a Bruker D8/SMART APEX II CCD diffractometer at 22 °C using ω scans. Structure solution and refinement were carried out with use of the SHELXTL (version 6.12) program package [12]. With the trigonal space group $P\bar{3}m1$ chosen, the initial atomic positions found by direct methods were consistent with the expected $CaAl_2Si_2$-type structure [13] and were standardized with the program STRUCTURE TIDY [14]. On the basis of the loaded composition and the EDX analysis, the single available transition-metal site was assumed to be occupied by 0.50 Cu and 0.50 Zn. Crystallographic details are summarized in Table 2. The cell parameters reported here for the single-crystal sample are slightly greater than those of the bulk powder prepared in the absence of I_2, suggesting that they may have small differences in composition; this observation is consistent with the occurrence of a solid solution in a different *RE* series, described later. Further data, in CIF format, have been sent to Fachinformationszentrum Karlsruhe, Abt. PROKA, 76344 Eggenstein-Leopoldshafen, Germany, as supplementary material no. CSD-422337 and can be obtained by contacting FIZ (quoting the article details and the corresponding CSD numbers).

Table 1
Cell parameters for *RE*CuZnP$_2$.

Compound	a (Å)	c (Å)	V (Å^3)	Reference
ScCuZnP$_2$	3.870(1)	6.312(2)	81.87(3)	[3i]
YCuZnP$_2$	3.983(1)	6.523(2)	89.62(3)	[3h,3i]
LaCuZnP$_2$	4.082(1)	6.742(2)	97.29(4)	[3i]
CeCuZnP$_2$	4.064(1)	6.697(2)	95.79(4)	[3i]
PrCuZnP$_2$	4.047(1)	6.661(1)	94.49(2)	This work
NdCuZnP$_2$	4.024(1)	6.615(2)	92.79(4)	This work
SmCuZnP$_2$	4.016(2)	6.592(2)	92.07(5)	[11]
GdCuZnP$_2$	3.994(1)	6.554(1)	90.38(2)	This work
TbCuZnP$_2$	3.990(1)	6.521(1)	89.90(2)	This work
DyCuZnP$_2$	3.979(1)	6.520(1)	89.41(2)	This work
HoCuZnP$_2$	3.968(1)	6.497(1)	88.57(2)	This work
ErCuZnP$_2$	3.958(1)	6.479(1)	87.88(2)	This work
TmCuZnP$_2$	3.936(1)	6.440(2)	86.39(3)	This work
YbCuZnP$_2$	3.946(1)	6.462(1)	87.14(1)	[3f]
LuCuZnP$_2$	3.924(1)	6.429(2)	85.76(4)	This work

Table 2
Crystallographic data for ErCuZnP$_2$.

Data collection and refinement	
Formula	ErCuZnP$_2$
Formula mass (amu)	358.11
Space group	$P\bar{3}m1$ (no. 164)
a (Å)	3.9469(3)
c (Å)	6.4636(4)
V (Å^3)	87.20(1)
Z	1
ρ_{calcd} (g cm^{-3})	6.819
Crystal dimensions (mm)	0.12 × 0.11 × 0.06
Radiation	Graphite monochromated Mo$K\alpha$, λ=0.71073 Å
μ(Mo$K\alpha$) (mm^{-1})	37.34
Transmission factors	0.082–0.238
2θ limits	$6.30^\circ \le 2\theta(\text{Mo}K\alpha) \le 65.78^\circ$
Data collected	$-5 \le h \le 5$, $-6 \le k \le 5$, $-9 \le l \le 9$
No. of data collected	1153
No. of unique data, including $F_o^2 < 0$	153 (R_{int}=0.023)
No. of unique data, with $F_o^2 > 2\sigma(F_o^2)$	153
No. of variables	10
$R(F)$ for $F_o^2 > 2\sigma(F_o^2)$[a]	0.012
$R_w(F_o^2)$[b]	0.029
Goodness of fit	1.19
$(\Delta\rho)_{max}$, $(\Delta\rho)_{min}$ (e Å^{-3})	2.28, −1.74
Positional and displacement parameters[c]	
Er at 1*a* (0, 0, 0)	
U_{eq} (Å^2)	0.0073(2)
M at 2*d* (1/3, 2/3, *z*)[d]	
z	0.6319(1)
U_{eq} (Å^2)	0.0120(2)
P at 2*d* (1/3, 2/3, *z*)	
z	0.2514(2)
U_{eq} (Å^2)	0.0068(2)
Interatomic distances (Å)	
Er–P (×6)	2.7987(7)
Er–*M* (×6)	3.2943(5)
M–P (×3)	2.4003(5)
M–P	2.4598(14)
M–*M* (×3)	2.8463(9)

[a] $R(F) = \sum \|F_o\| - |F_c\| / \sum |F_o|$.

[b] $R_w(F_o^2) = \left[\sum[w(F_o^2 - F_c^2)^2] / \sum wF_o^4\right]^{1/2}$; $w^{-1} = [\sigma^2(F_o^2) + (0.0108p)^2 + 0.2664p]$, where $p = [\max(F_o^2, 0) + 2F_c^2]/3$.

[c] U_{eq} is defined as one-third of the trace of the orthogonalized U_{ij} tensor.

[d] Occupancies of 0.50 Cu and 0.50 Zn.

2.3. Band structure calculations

Tight-binding linear muffin tin orbital (TB-LMTO) band structure calculations were performed within the local density and atomic spheres approximation with use of the Stuttgart TB-LMTO program [15]. To circumvent difficulties associated with the description of 4*f* orbitals and to treat the mixed occupancy of the transition-metal site, an ordered model based on YCuZnP$_2$ was examined in which Cu and Zn atoms are placed in separate sites: space group *P*3*m*1 (no. 156); Y, 1*a* (0, 0, 0); Cu, 1*b* (1/3, 2/3, 0.368); Zn, 1*c* (2/3, 1/3, 0.632); P1, 1*b* (1/3, 2/3, 0.749); P2, 1*c* (2/3, 1/3, 0.251). In this idealized ordered model, there are Cu–Zn contacts but no Cu–Cu or Zn–Zn contacts. The basis set consisted of Y 5*s*/5*p*/4*d*/4*f*, Cu 4*s*/4*p*/3*d*, Zn 4*s*/4*p*/3*d*, and P 3*s*/3*p*/3*d* orbitals, with the Y 4*f* and P 3*d* orbitals being downfolded. Integrations in reciprocal

space were carried out with an improved tetrahedron method over 248 irreducible *k* points within the first Brillouin zone. A similar calculation was repeated for $LaCuZnP_2$ to explore the effect of changing the *RE* component.

2.4. X-ray photoelectron spectroscopy

XPS spectra for *RE*$CuZnP_2$ (*RE*=Gd–Er) were collected on a Kratos AXIS 165 spectrometer equipped with a monochromatic Al*K*α source (15 kV, 14 mA) and a hybrid lens with a spot size of 700 μm × 400 μm. Because the samples are air-stable, no special precautions were necessary for handling. Samples were ground into fine powder, pressed onto In foil, mounted onto a Cu sample holder, and transferred to the XPS instrument. The pressure inside the analysis chamber was maintained at 10^{-7}–10^{-9} Pa. The samples were sputter-cleaned with an Ar^+ ion beam (4 kV, 10 mA) until all surface oxides were removed. This sputtering procedure caused a slight reduction in P, noticeable in the P 2*p* XPS spectra, which are not presented.

Survey spectra, which were collected with a binding energy (BE) range of 0 − 1100 eV, a pass energy of 160 eV, a step size of 0.7 eV, and a sweep time of 180 s, confirmed the expected compositions. In particular, the Cu:Zn ratio was clearly different in the survey spectra for $GdCuZnP_2$ and $GdCu_{1.3}Zn_{0.7}P_2$, two members chosen for study from the $GdCu_xZn_{2-x}P_2$ solid solution. High-resolution spectra of the valence band and the Cu 2*p* core-lines were collected with energy envelopes of 30 and 70 eV, respectively. No charge correction was needed. All spectra, calibrated against the C 1*s* line at 284.8 eV arising from adventitious carbon, were analyzed with the use of the CasaXPS software package [16]. The background, which arises from electron energy loss, was removed by applying a Shirley-type function. The precision in BE values is estimated to be ± 0.1 eV, on the basis of previous measurements made on this instrument.

2.5. Magnetic measurements

Measurements of dc magnetic susceptibility were made on *RE*$CuZnP_2$ (*RE*=Gd–Er) (~150 mg each), for which pure samples were available, under an applied field of 0.5 T from 5 to 300 K on a Quantum Design 9T-PPMS dc magnetometer/ac susceptometer. Values of magnetic susceptibility were corrected from contributions from the holder and underlying sample core diamagnetism.

3. Results and discussion

3.1. Crystal structure

Ternary pnictides with the $CaAl_2Si_2$-type structure are normally restricted to compounds AB_2Pn_2 in which *A* and *B* are divalent metals, thereby limiting the previously known rare-earth representatives to those containing Eu and Yb [3–5]. The versatility of this structure type can be considerably expanded to include trivalent *RE* metals as the *A* component, by compensating with a mixture of monovalent and divalent metals for the *B* component. In this way, the quaternary phosphides *RE*$CuZnP_2$ can be formed for nearly all *RE* metals, including Sc and Y. There is evidence, presented later, that these phosphides may exhibit some solid solubility, *RE*$Cu_xZn_{2-x}P_2$, but for simplicity we assume the idealized formula *RE*$CuZnP_2$ (with $x=1$) in subsequent discussion. The new compounds prepared here (Table 1) integrate well into the existing series [3f,3h,3i,11], with the cell parameters varying smoothly through the lanthanide members (Fig. 1). (The deviation seen for the Yb member may be attributed to the occurrence of mixed valence if the composition is slightly off-stoichiometry, with magnetic measurements providing evidence for increasing amounts of divalent Yb with Zn-richer content in the solid solutions $YbCu_xZn_{2-x}P_2$ [6a].)

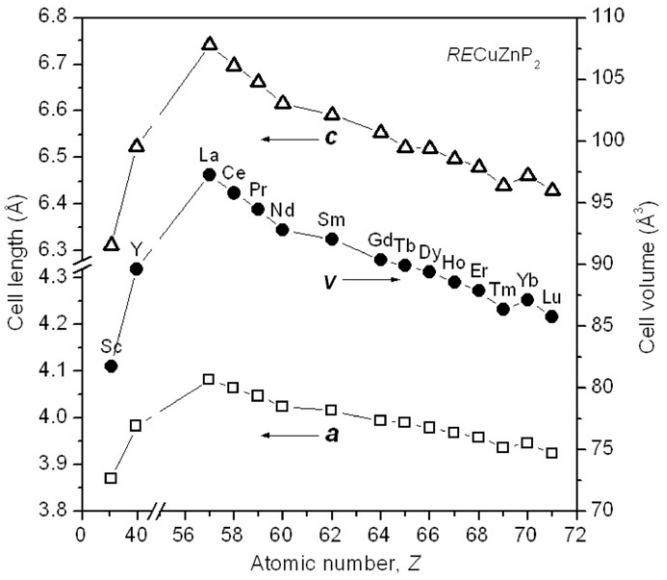

Fig. 1. Plot of cell parameters for *RE*$CuZnP_2$.

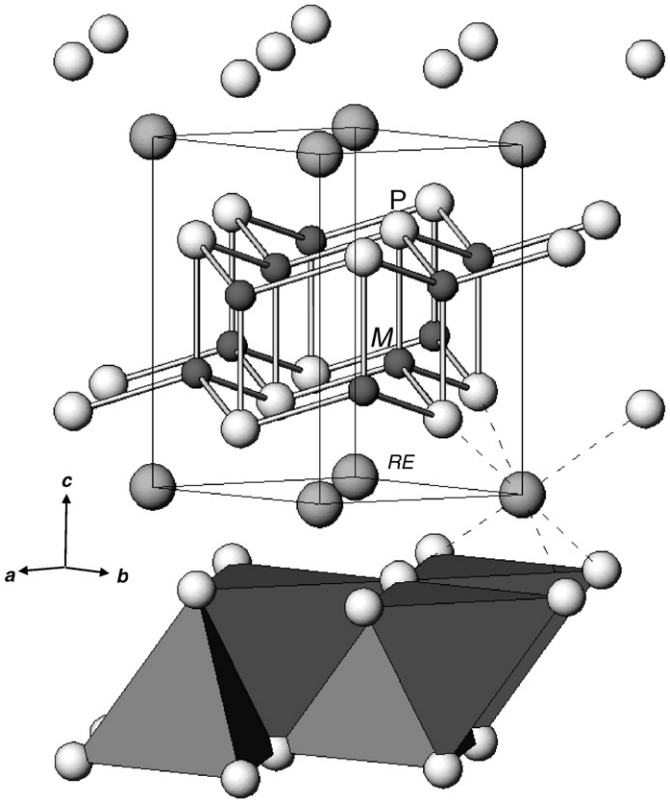

Fig. 2. Structure of *RE*$CuZnP_2$, highlighting either the $[M_2P_2]$ double layers (*M*=Cu and Zn) alternately stacked with nets of *RE* atoms, or the coordination polyhedra around the *RE* and *M* atoms.

The trigonal structure of *RE*$CuZnP_2$ can be described in several ways. It consists of a stacking along the *c*-direction of hexagonal nets of RE^{3+} cations alternating with $[M_2P_2]^{3-}$ double layers (where *M*=Cu and Zn), which are built up of puckered hexagonal nets (Fig. 2). Within the hcp arrangement of P atoms, the *RE* atoms

occupy half the octahedral sites and *M* atoms occupy half the tetrahedral sites. In terms of a polyhedral representation, two types of slabs parallel to the *ab* plane are formed by either edge-sharing REP_6 octahedra or by edge-sharing MP_4 tetrahedra, respectively. Structural relationships to other types, such as wurtzite, $BaAl_4$, and $CaSi_2$, have been well described in the literature [10]. In $ErCuZnP_2$, for which a single-crystal structure determination was performed, the vertical *M*–P bond (2.4598(14) Å) is longer than the three lateral *M*–P bonds (2.4003(5) Å), in agreement with theoretical expectations for $CaAl_2Si_2$-type structures consisting of d^0 or d^{10} metals as the *B* component [10a,10d]. The *M*–*M* separation of 2.8463(9) Å is 0.5 Å longer than the sum of the metallic radii (Pauling R_1 values of 1.18 Å for Cu and 1.21 Å for Zn) [17], but it is worthwhile inquiring whether any weak interaction occurs even at this distance.

3.2. Electronic structure

As in nearly all $CaAl_2Si_2$-type phases, the compounds $RECuZnP_2$ satisfy the Zintl–Klemm formalism in being charge-balanced. With a count of exactly 16 valence electrons, the formulation $RE^{3+}Cu^{1+}Zn^{2+}(P^{3-})_2$ implies closed-shell configurations for all atoms and, in principle, the presence of a band gap in the solid. We test these predictions through a band structure calculation on $YCuZnP_2$ and through measurements of the experimental valence band spectra for several $RECuZnP_2$ members.

Remarkably, the density of states (DOS) curve for a hypothetically ordered $YCuZnP_2$ model indicates a semimetal; i.e., the valence and conduction bands just touch so that the band gap vanishes (Fig. 3a), with the top of the valence band at Γ (0, 0, 0) and the bottom of the conduction band at L (1/2, 0, 1/2) (Fig. S3 in Supplementary Data). (At the Fermi level, the DOS is about 0.05 states/eV per cell.) Consistent with the d^{10} configuration of the *M* atoms, essentially all of their *d*-states are located below the Fermi level, dispersed from −6 to 0 eV for Cu and more localized from −9 to −8 eV for Zn (similar to features previously seen in the DOS curves for LaZnAsO and YZnAsO) [18]. There is significant mixing of the Cu 3*d* and P 3*p* states from −6 to 0 eV. Interestingly, some Y-based states are also found below the Fermi level, suggesting their participation in bonding, as anticipated by the demonstration that Ca atoms are non-innocent in $CaAl_2Si_2$ itself [10d]. The crystal orbital Hamilton population (COHP) curves (Fig. 3b) indicate that all *M*–P and Y–P bonding levels are filled up to the Fermi level, this optimization in bonding being characteristic of Zintl phases. The average integrated COHP values (–ICOHP) for the each of the three shorter lateral *M*–P bonds (2.09 eV/bond) is greater than for the longer vertical *M*–P bond (1.45 eV/bond). For the Y–P bond, the –ICOHP value is smaller (1.28 eV/bond). Finally, the occupation of very weakly bonding *M*–*M* levels (corresponding here to Cu–Zn contacts in an idealized ordered model) leads to a small but not negligible –ICOHP value of 0.23 eV/bond, involving overlap of mostly *M* 4*s* orbitals.

Although the feature of a vanishing band gap in $YCuZnP_2$ seems to be quite surprising at first glance, it agrees with the proposal that the band gap should diminish with a smaller difference in electronegativity between the *B* and *X* atoms within the $[B_2X_2]$ double layer in $CaAl_2Si_2$-type phases AB_2X_2 [10d]. For example, previous calculations (in which the *A* components are included) show a 1 eV band gap in $BaMg_2Sb_2$ [10d] and a 0.5 eV band gap in $EuMg_2Sb_2$ [6c] (for which the difference in Pauling electronegativity, $\Delta\chi$, is 0.7), in contrast to zero band gaps in $CaAl_2Si_2$ [8a] and $YbAl_2Si_2$ [8b] ($\Delta\chi = 0.3$) as well as in $CaAl_2Ge_2$ [8c] ($\Delta\chi = 0.4$). In fact, for $CaAl_2Si_2$ itself, the absence of a band gap is dominated by the small electronegativity difference between Al and Si, with the Ca atoms playing a minor role [10d]. The tendency towards metallic behavior in these 16-electron $CaAl_2Si_2$-type phases is thus different in origin from the case of the few 17-electron representatives such as $REAl_2Ge_2$ that derive their metallic properties by virtue of the conduction band already being partially filled [8c]. If the average electronegativity of Cu and Zn is taken, $\Delta\chi$ is 0.4 in $YCuZnP_2$, similar to those in the zero-band-gap cases above. Accordingly, the electrical resistivities of $SmCuZnP_2$ and related $REAgZnP_2$ (RE = La, Sm) compounds were previously found to be large (0.1–0.2 Ω cm) and to have temperature dependences suggestive of highly degenerate (heavily doped) semiconductors, whose behavior is similar to semimetals [11].

Although the size of the band gap is primarily controlled by intralayer effects (i.e. difference in electronegativity between *B* and *X* in AB_2X_2), it also depends secondarily on the nature of the *A* component, as was demonstrated in the series AZn_2Sb_2 (A = Sr, Ca, Yb, Eu) [7b]. Changing the *A* component introduces not only a size effect, but also modifies the density of states near the Fermi level through interactions with the other atoms. That is, the *RE* cations in $RECuZnP_2$ do not merely act as spacers between layers, but participate in weak bonding, as was seen above in the modest Y–P interactions in $YCuZnP_2$. At the other extreme, for a large *RE* atom in $RECuZnP_2$, the DOS curve for a hypothetically ordered $LaCuZnP_2$ model reveals that a band gap of about 0.2 eV opens up and that essentially no La states appear below the Fermi level (Figs. S3 and S4 in Supplementary Data).

3.3. XPS analysis

Further experimental evidence for the electronic structure of $RECuZnP_2$ may be sought through their XPS spectra. All the valence

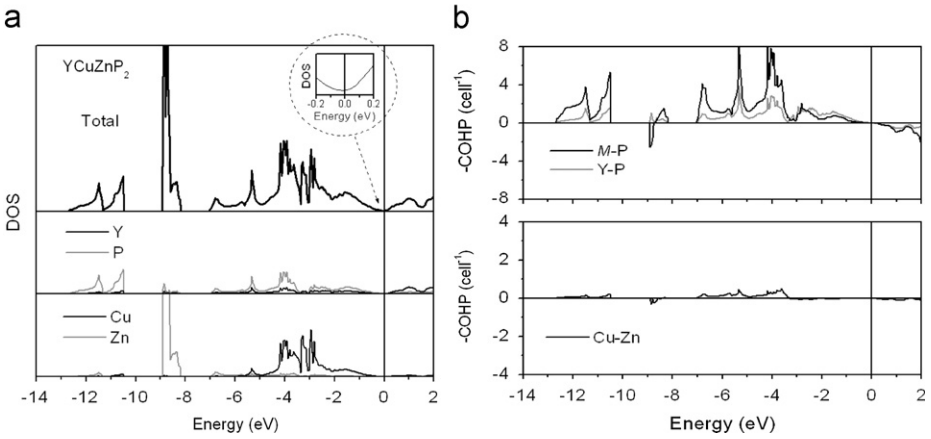

Fig. 3. (a) Density of states (DOS) and its atomic projections for a hypothetically ordered $YCuZnP_2$ model with the $CaAl_2Si_2$-type structure. (b) Crystal orbital Hamilton population (–COHP) curves for *M*–P, Y–P, and Cu–Zn contacts. The Fermi level is at 0 eV.

band spectra (for *RE*=Gd–Er) show a smooth dropoff up to the Fermi energy (Fig. 4). This behavior does not correspond to typical metals, for which the spectra should show finite intensity and a clean cut-off at the Fermi edge (as seen in Ni_2P, for example) [19], with the first derivative reaching a maximum [20]. Rather, the absence of states at the Fermi edge implies a semiconductor with a band gap, in this case, a vanishingly small one. Indeed, the line-shapes of the spectra near the Fermi edge resemble closely the curvature in the calculated DOS curve for $YCuZnP_2$ (Fig. 3a), although it is important to bear in mind that different photo-ionization cross-sections also influence the XPS intensities [21]. The spectra exhibit three characteristic features (labeled A–C) which can be interpreted with the aid of the DOS curve and its projections. Peak A, comprising mostly Cu 3*d* and P 3*p* states, spreads over 0–6 eV in BE. Peak B, comprising mostly Zn 3*d* states, spreads over 8–14 eV in BE, as is commonly found in the valence band spectra of compounds containing Zn^{2+} [22]. Although P 3*s* states should also be found in this region, they are likely buried because of their smaller photoionization cross-sections relative to the Zn 3*d* states [21]. Peak A and, to a lesser extent, peak B remain relatively invariant in their positions and lineshapes, consistent with the minor changes expected in the $[M_2P_2]$ double layer as the *RE* component is varied. In contrast, peak C shifts dramatically in BE for different *RE*$CuZnP_2$ members, indicating that it corresponds to the *RE* 4*f* states. Common in the spectra of many rare-earth-containing compounds [23,24], multiplet splitting of the *RE* 4*f* states complicates the interpretation and leads to no obvious trends in the positions of these states. In the spectra of $HoCuZnP_2$ and $ErCuZnP_2$, the substantial broadening of peak C may be attributed to multiplet-split *RE* 4*f* states overlapping with the Zn 3*d* states.

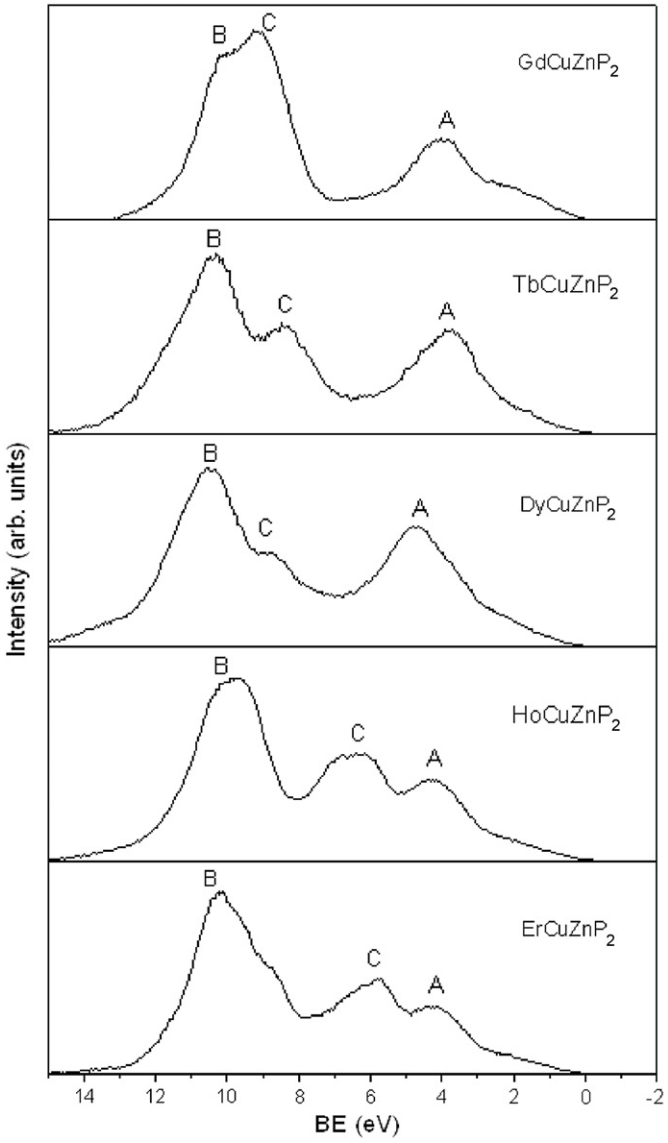

Fig. 4. XPS valence band spectra for *RE*$CuZnP_2$ (*RE*=Gd–Er). Assignments of peaks labeled A, B, and C are given in the text.

3.4. $GdCu_xZn_{2-x}P_2$ solid solution

The occurrence of a zero band gap in the calculated DOS curve for $YCuZnP_2$ presents an opportunity to test whether the $CaAl_2Si_2$-type structure can be retained when the electron count is changed, through formation of a solid solution. Examples where this has been previously achieved have been limited to decreasing the electron count in $GdMn_xAl_{2-x}Si_2$ ($0 \le x \le 0.25$) [8a] and $GdZn_xAl_{2-x}Ge_2$ ($0 \le x \le 1.0$) [8c], which start off intrinsically metallic at 17 electrons per formula unit, or to inducing mixed valence (Yb^{II}–Yb^{III}) in $YbCu_xZn_{2-x}P_2$ and $YbCu_xZn_{2-x}As_2$ ($0 \le x \le 1.0$) [6a].

Choosing the $GdCu_xZn_{2-x}P_2$ series to examine, we were successful in establishing a solid solubility range for $1.0 \le x \le 1.3$, the cell parameters increasing with greater proportion of Cu atoms (Fig. 5). Because Gd must be exclusively trivalent, an increase in *x* implies that either the Fermi level will be lowered because of the decreased electron count, or more improbably, some Cu^{2+} species are present to restore charge balance. In the absence of electrical resistivity data (for want of suitably sized crystals), the valence band XPS spectra of $GdCuZnP_2$ and $GdCu_{1.3}Zn_{0.7}P_2$ are compared (Fig. 6a). If the assignments of XPS features discussed above are extended to $GdCu_{1.3}Zn_{0.7}P_2$, the lower intensity around 10 eV in BE implies fewer Zn 3*d* states, in agreement with the reduced Zn concentration. The lower intensity near the Fermi edge (down to 3 eV) is attributed to hole-doping of the valence band, a result of the reduced electron count.

To rule out the presence of Cu^{2+}, the Cu 2*p* core-line XPS spectra for $GdCuZnP_2$ and $GdCu_{1.3}Zn_{0.7}P_2$ can be inspected (Fig. 6b). The two spectra are identical to each other and, in fact, to all other *RE*$CuZnP_2$ members examined (Fig. S5 in Supplementary Data). The

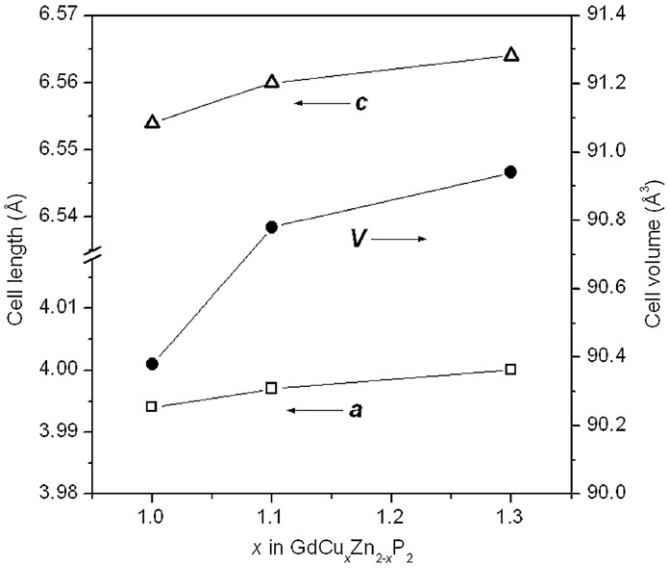

Fig. 5. Plot of cell parameters vs. *x* for $CaAl_2Si_2$-type phase formed in $GdCu_xZn_{2-x}P_2$ solid solution.

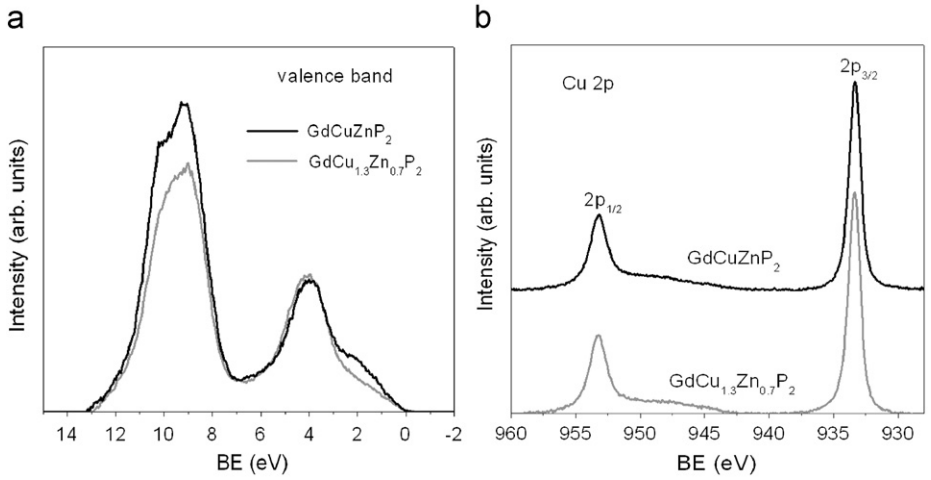

Fig. 6. (a) XPS valence band spectra for $GdCuZnP_2$ and $GdCu_{1.3}Zn_{0.7}P_2$, normalized to the peak at 4 eV and overlapped to highlight the intensity differences at 10 eV and near the Fermi edge. (b) Comparison of Cu 2*p* XPS spectra for $GdCuZnP_2$ and $GdCu_{1.3}Zn_{0.7}P_2$.

two peaks represent the $2p_{3/2}$ and $2p_{1/2}$ spin–orbit-coupled final states, in an intensity ratio of 2:1 and each with a full-width-at-half-maximum (FWHM) of about 1.1 eV. The Cu $2p_{3/2}$ BE for all these compounds is 933.4 eV, which is greater than that for elemental Cu (932.86(4) eV) [25]. Unfortunately, the oxidation state of Cu is not easily correlated with the Cu $2p_{3/2}$ BEs, which are typically similar for Cu^{1+} and Cu^0 species but usually higher for Cu^{2+} species [26]. The lineshape and FWHM do tend to resemble those in compounds containing Cu^{1+} (e.g., 1.0 eV in ZrCuSiP) [25] but not Cu^{2+} (e.g., 1.6 eV in $CuBr_2$) [27]. However, the key distinguishing feature is a small satellite found between 945 and 940 eV that is characteristic of Cu^{2+} but not Cu^{1+} or Cu^0 systems [28]. (This satellite has been proposed to arise from either a shake-up process in which Cu valence electrons are excited into the conduction band after photoionization, or a shake-down process in which ligand electrons relax into the Cu-based conduction states; both theories predict the occurrence of such a satellite only when empty Cu 3*d* states are available [26,28].) The absence of such a satellite in the collected spectra further supports the assertion that increasing the Cu concentration in $GdCu_xZn_{2-x}P_2$ leads to a lowering of the Fermi level in the valence band, with the local electronic environment around Cu remaining unchanged.

3.5. Magnetic properties

The compounds *RE*$CuZnP_2$ (*RE*=Gd–Er), as well as $GdCu_{1.3}Zn_{0.7}P_2$, exhibit paramagnetic behavior (Fig. S6 in Supplementary Data). The inverse magnetic susceptibility curves are linear down to relatively low temperatures (Fig. 7). No long-range ordering sets in within the temperatures measured, but a downturn in the magnetic susceptibility appears to be imminent in some cases, such as $TbCuZnP_2$, below 5 K. Fitting of the linear portion of the inverse magnetic susceptibility curves to the Curie–Weiss law, $\chi = C/(T-\theta_p)$, yields effective magnetic moments (derived from the Curie constants through $\mu_{eff}=(8C)^{1/2}$) that are slightly larger but otherwise in good agreement with the theoretical free-ion values for the trivalent RE^{3+} species (Table 3). The contribution of additional local moments from Cu and Zn atoms is unlikely, given the XPS evidence above for only Cu^{1+} species and given the fact that the magnetic properties of $GdCuZnP_2$ and $GdCu_{1.3}Zn_{0.7}P_2$ are not significantly different. The Weiss parameters, θ_p, are all positive and almost follow de Gennes scaling, suggesting that conduction electrons may play a mediating role in the magnetic coupling

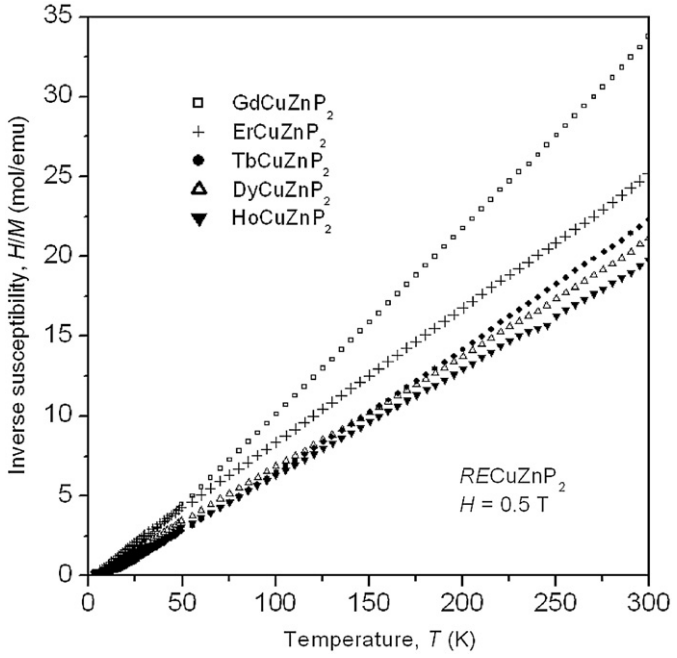

Fig. 7. Plots of inverse magnetic susceptibility vs. temperature for *RE*$CuZnP_2$ (*RE*=Gd–Er).

Table 3
Magnetic data for *RE*$CuZnP_2$.

Compound	θ_p (K)	$\mu_{eff,\ meas}$ (μ_B/f.u.)	$\mu_{eff,\ theor}$ for RE^{3+} (μ_B)
$GdCuZnP_2$	12.8(3)	8.29(1)	7.94
$GdCu_{1.3}Zn_{0.7}P_2$	11.8(3)	8.13(1)	7.94
$TbCuZnP_2$	15.4(4)	10.17(1)	9.72
$DyCuZnP_2$	6.2(2)	10.79(1)	10.64
$HoCuZnP_2$	5.2(2)	10.96(1)	10.61
$ErCuZnP_2$	0.3(2)	9.78(1)	9.58

interactions. We note that the magnetic susceptibility of $YbCuZnP_2$ has been previously reported to follow the Curie–Weiss law, but with a pronounced negative Weiss parameter of −108 K [6a].

4. Conclusions

The versatility of the $CaAl_2Si_2$-type structure has been demonstrated through the preparation of the quaternary rare-earth representatives *RE*$CuZnP_2$, which form for all *RE* metals (except Pm and Eu). Despite being charge-balanced and thus Zintl phases, the electronic structure is that of a semimetal, a consequence of the moderately small electronegativity difference between Cu/Zn and P atoms, with a vanishingly small band gap in the case of the later *RE* members. The structure can then be retained even with a change in electron count, as exemplified by the formation of a solid solution in $GdCu_xZn_{2-x}P_2$. Band structure calculations suggest that the *RE* atoms may participate in some degree of *RE*–P bonding, supporting earlier assertions about the contribution of the *A* cation in $CaAl_2Si_2$-type phases AB_2X_2 to the electronic structure [10d], the importance diminishing with larger *RE* atoms. (It would be interesting, for example, to ascertain if any solid solubility occurs in $LaCu_xZn_{2-x}P_2$, or for that matter, any of the other *RE* members.) XPS spectra confirm that the local electronic environments around Cu and Zn atoms are unchanged with *RE* substitution and with greater Cu concentrations. Rather, a decrease in electron count is accommodated by lowering of the Fermi level in the valence band. The compounds *RE*$CuZnP_2$ (*RE*=Gd–Er) are paramagnetic, with no long-range ordering apparent down to 5 K.

Acknowledgments

This work was supported by the Natural Sciences and Engineering Research Council of Canada (NSERC). P.E.R.B. acknowledges NSERC, Alberta Ingenuity, and the University of Alberta for scholarship support. We thank Dr. Robert McDonald and Dr. Michael J. Ferguson (X-ray Crystallography Laboratory) for assistance with the single-crystal X-ray data collection, and Ms. Christina Barker (Department of Chemical and Materials Engineering) and Ms. DeAnn Rollings (Department of Earth and Atmospheric Sciences) for the EDX analyses. Access to the Kratos AXIS 165 XPS spectrometer was provided by the Alberta Centre for Surface Engineering and Science, which was established with support from the Canada Foundation for Innovation and Alberta Innovation and Science.

Appendix A. Supplementary materials

Supplementary data associated with this article can be found in the online version at doi:10.1016/j.jssc.2010.11.001.

References

[1] C. Zheng, R. Hoffmann, J. Solid State Chem. 72 (1988) 58–71.
[2] D. Mandrus, A.S. Sefat, M.A. McGuire, B.C. Sales, Chem. Mater. 22 (2010) 715–723.
[3] (a) A. Mewis, P. Klüfers, H.-U. Schuster, Z. Naturforsch. B 30 (1975) 132;
(b) P. Klüfers, A. Mewis, Z. Naturforsch. B 32 (1977) 353–354;
(c) P. Klüfers, A. Mewis, Z. Naturforsch. B 32 (1977) 753–756;
(d) A. Mewis, Z. Naturforsch. B 33 (1978) 382–384;
(e) A. Mewis, Z. Naturforsch. B 33 (1978) 606–609;
(f) P. Klüfers, A. Mewis, H.-U. Schuster, Z. Kristallogr. 149 (1979) 211–225;
(g) A. Mewis, Z. Naturforsch. B 35 (1980) 939–941;
(h) P. Klüfers, H. Neumann, A. Mewis, H.-U. Schuster, Z. Naturforsch. B 35 (1980) 1317–1318;
(i) A. Mahan, A. Mewis, Z. Naturforsch. B 38 (1983) 1041–1045;
(j) P. Klüfers, A. Mewis, Z. Kristallogr. 169 (1984) 135–147;
(k) A. Artmann, A. Mewis, M. Roepke, G. Michels, Z. Anorg. Allg. Chem. 622 (1996) 679–682.
[4] K. Deller, B. Eisenmann, Z. Naturforsch. B 32 (1977) 612–616.
[5] R. Rühl, W. Jeitschko, Mater. Res. Bull. 14 (1979) 513–517.
[6] (a) G. Zwiener, H. Neumann, H.-U. Schuster, Z. Naturforsch. B 86 (1981) 1195–1197;
(b) A. Nateprov, J. Cisowski, J. Heimann, I. Mirebeau, J. Alloys Compd. 290 (1999) 6–9;
(c) F. Wartenberg, C. Kranenberg, R. Pocha, D. Johrendt, A. Mewis, R.-D. Hoffmann, B.D. Mosel, R. Pöttgen, Z. Naturforsch. B 57 (2002) 1270–1276;
(d) A.C. Payne, A.E. Sprauve, M.M. Olmstead, S.M. Kauzlarich, J.Y. Chan, B.A. Reisner, J.W. Lynn, J. Solid State Chem. 163 (2002) 498–505;
(e) S. Bobev, J. Merz, A. Lima, V. Fritsch, J.D. Thompson, J.L. Sarrao, M. Gillessen, R. Dronskowski, Inorg. Chem. 45 (2006) 4047–4054;
(f) A.V. Morozkin, O. Isnard, P. Henry, S. Granovsky, R. Nirmala, P. Manfrinetti, J. Alloys Compd. 420 (2006) 34–36;
(g) I. Schellenberg, M. Eul, W. Hermes, R. Pöttgen, Z. Anorg. Allg. Chem. 636 (2010) 85–93.
[7] (a) S.M. Kauzlarich, C.L. Condron, J.K. Wassei, T. Ikeda, G.J. Snyder, J. Solid State Chem. 182 (2009) 240–245;
(b) E.S. Toberer, A.F. May, B.C. Melot, E. Flage-Larsen, G.J. Snyder, Dalton Trans. 39 (2010) 1046–1054;
(c) H. Zhang, M. Baitinger, M.-B. Tang, Z.-Y. Man, H.-H. Chen, X.-X. Yang, Y. Liu, L. Chen, Y. Grin, J.-T. Zhao, Dalton Trans. 39 (2010) 1101–1104;
(d) Q.-G. Cao, H. Zhang, M.-B. Tang, H.-H. Chen, X.-X. Yang, Y. Grin, J.-T. Zhao, J. Appl. Phys. 107 (2010) 053714-1–053714-5.
[8] (a) C. Kranenberg, D. Johrendt, A. Mewis, Z. Anorg. Allg. Chem. 625 (1999) 1787–1793;
(b) C. Kranenberg, D. Johrendt, A. Mewis, R. Pöttgen, G. Kotzyba, C. Rosenhahn, B.D. Mozel, Solid State Sci. 2 (2000) 215–222;
(c) C. Kranenberg, D. Johrendt, A. Mewis, Solid State Sci. 4 (2002) 261–265.
[9] M. Imai, H. Abe, K. Yamada, Inorg. Chem. 43 (2004) 5186–5188.
[10] (a) C. Zheng, R. Hoffmann, R. Nesper, H.-G. von Schnering, J. Am. Chem. Soc. 108 (1986) 1876–1884;
(b) J.K. Burdett, G.J. Miller, Chem. Mater. 2 (1990) 12–26;
(c) S.L. Brock, J.E. Greedan, S.M. Kauzlarich, J. Solid State Chem. 109 (1994) 416–418;
(d) P. Alemany, M. Llunell, E. Canadell, J. Comput. Chem. 29 (2008) 2144–2153.
[11] P. Tejedor, A.M. Stacy, J. Solid State Chem. 89 (1990) 227–236.
[12] G.M. Sheldrick, SHELXTL, version 6.12, Bruker AXS Inc., Madison, WI, 2001.
[13] E.I. Gladyshevskii, P.I. Kripyakevich, O.I. Bodak, Ukr. Fiz. Zh. 12 (1967) 447–452.
[14] L.M. Gelato, E. Parthé, J. Appl. Crystallogr. 20 (1987) 139–143.
[15] R. Tank, O. Jepsen, A. Burkhardt, O.K. Andersen, TB-LMTO-ASA Program, version 4.7, Max Planck Institut für Festkörperforschung, Stuttgart, Germany, 1998.
[16] N. Fairley, CasaXPS, version 2.3.9, Casa Software Ltd., Teighnmouth, Devon, UK, 2003, 〈http://www.casaxps.com〉.
[17] L. Pauling, The Nature of the Chemical Bond, 3rd ed., Cornell University Press, Ithaca, NY, 1960.
[18] V.V. Bannikov, I.R. Shein, A.L. Ivanovskii, Mater. Chem. Phys. 116 (2009) 129–133.
[19] K. Edamoto, Y. Nakadai, H. Inomata, K. Ozawa, S. Otani, Solid State Commun. 148 (2008) 135–138.
[20] D. Briggs, M. P. Seah (Eds.), Practical Surface Analysis, vol. 1, Auger and X-ray Photoelectron Spectroscopy, 2nd ed. Wiley, Chichester, UK, 1990.
[21] (a) J.J. Yeh, I. Lindau, At. Data Nucl. Data Tables 32 (1985) 1–155;
(b) J.H. Scofield, J. Electron Spectrosc. Relat. Phenom. 8 (1976) 129–137.
[22] C.D. Wagner, A.V. Naumkin, A. Kraut-Vass, J.W. Allison, C.J. Powell, J.R. Rumble Jr., NIST X-ray Photoelectron Spectroscopy Database, version 3.5 (web version), National Institute of Standards and Technology, Gaithersburg, MD, 2003, 〈http://srdata.nist.gov/xps〉.
[23] G.P. Nizhnikova, O.V. Farberovich, Phys. Status Solidi B 155 (1989) 491–500.
[24] M. Drzyzga, J. Szade, J. Deniszczyk, T. Michalecki, J. Phys.: Condens. Matter 15 (2003) 3701–3716.
[25] P.E.R. Blanchard, R.G. Cavell, A. Mar, J. Solid State Chem. 183 (2010) 1536–1544.
[26] (a) D.C. Frost, A. Ishitani, C.A. McDowell, Mol. Phys. 24 (1972) 861–877;
(b) S.K. Chawla, N. Sankarraman, J.H. Payer, J. Electron Spectrosc. Relat. Phenom. 61 (1992) 1–18;
(c) A. Roberts, D. Engelberg, Y. Liu, G.E. Thompson, M.R. Alexander, Surf. Interface Anal. 33 (2002) 697–703.
[27] R.P. Vasquez, Surf. Sci. Spectra 2 (1994) 165–169.
[28] (a) A. Rosencwaig, G.K. Wertheim, J. Electron Spectrosc. Relat. Phenom. 1 (1972/73) 493–496;
(b) P.C. Healy, S. Myhra, A.M. Stewart, Jpn. J. Appl. Phys. 26 (1987) L1884–L1887.